5938–5950 *Nucleic Acids Research, 2012, Vol. 40, No. 13* *Published online 24 March 2012*
doi:10.1093/nar/gks265

Interactions between DNA, transcriptional regulator Dreb2a and the Med25 mediator subunit from *Arabidopsis thaliana* involve conformational changes

Jeanette Blomberg[1], Ximena Aguilar[2], Kristoffer Brännström[1], Linn Rautio[1], Anders Olofsson[1], Pernilla Wittung-Stafshede[2] and Stefan Björklund[1,*]

[1]Department of Medical Biochemistry and Biophysics and [2]Department of Chemistry, Umeå University, SE-901 87 Umeå, Sweden

Received November 29, 2011; Revised March 8, 2012; Accepted March 9, 2012

ABSTRACT

Mediator is a multiprotein coregulatory complex that conveys signals from DNA-bound transcriptional regulators to the RNA polymerase II transcription machinery in eukaryotes. The molecular mechanisms for how these signals are transmitted are still elusive. By using purified transcription factor Dreb2a, mediator subunit Med25 from *Arabidopsis thaliana*, and a combination of biochemical and biophysical methods, we show that binding of Dreb2a to its canonical DNA sequence leads to an increase in secondary structure of the transcription factor. Similarly, interaction between the Dreb2a and Med25 in the absence of DNA results in conformational changes. However, the presence of the canonical Dreb2a DNA-binding site reduces the affinity between Dreb2a and Med25. We conclude that transcription regulation is facilitated by small but distinct changes in energetic and structural parameters of the involved proteins.

INTRODUCTION

Eukaryotic cells express a set of general transcription factors (GTFs: TBP, TFIIB, TFIIE, TFIIF and TFIIH) and RNA polymerase II, which are required for transcription of all protein-encoding genes. Together, the GTFs form a so called pre-initiation complex (PIC) that assembles close to the transcription start site. Transcription is regulated at several levels; most importantly by changes in chromatin structure and by transcriptional regulators (activators or repressors) that bind to specific DNA sequences. In the latter process, transcriptional regulators execute their function by affecting different steps in transcription such as formation of the PIC (1,2), promoter escape (3) and elongation (4–6). There are several examples of direct interactions between DNA-bound transcriptional regulators and components of the general transcription machinery, but these interactions are not sufficient to support regulated transcription. Instead, transcriptional regulators operate through interactions with different types of coregulators (coactivators and corepressors), which transmit signals to the general transcription machinery. Coregulators are not believed to interact with DNA, but rather to form bridges between the DNA-bound activators/repressors and the GTFs. The most important coregulator is mediator, a multisubunit protein complex which is required for proper expression of nearly all genes in all eukaryotes (7). Mediator was initially identified in yeast (8,9), but it is now clear that mediator is present in all eukarya and a common terminology for mediator subunits in all species has been proposed (10,11)

Even though the subunit composition and the structure of mediator are well described, less is known about how mediator operates to integrate and convey signals from DNA-bound transcriptional regulators. This is in part due to its complexity and size. Direct interactions between transcriptional regulators and different mediator subunits are believed to recruit and stabilize mediator at the promoter, and there are indications that interactions with transcriptional regulators induce conformational changes or structural shifts in mediator (12–14). It is possible that such conformational changes in mediator are propagated to induce further structural shifts in components of the general transcription machinery. These changes, combined with other signal pathways that cause posttranslational modifications of different

*To whom correspondence should be addressed. Tel: +46 90 7866788; Fax: +46 90 7869795; Email: stefan.bjorklund@medchem.umu.se

transcription factors, might therefore determine the level of transcription from each gene.

We recently identified mediator in *Arabidopsis thaliana* and we have also reported that the Med25 subunit in *Arabidopsis* interacts with three different transcription factors, Dreb2a, Zfhd1 and myb-like which all are involved in different stress response pathways (15,16) In this article, we use a set of biochemical and biophysical methods to study interaction between the Med25 mediator subunit and the transcription factor Dreb2a from *A. thaliana*. We also investigate how this interaction is affected by the presence of the cognate DNA-binding site for Dreb2a. Our results show that functional interactions between Dreb2a and Med25 induce conformational changes which in turn cause changes in their binding affinity.

MATERIALS AND METHODS

Protein purification and expression

Purification of $Med25_{551–680}$ and $Dreb2a_{168–335}$ was carried out as described previously (16). The GST-tag of $Med25_{551–680}$ that is removed by cleavage with Prescission Enzyme (GE Healthcare) was collected and stored in −20°C before use as a control for the experiments described in Figure 7. The nucleotide sequence corresponding to amino acids 168–253 ($Dreb2a_{168–253}$) and 254–335 ($Dreb2a_{254–335}$) was amplified from cDNA with polymerase chain reaction and cloned into the NcoI/NotI sites of the pETM-6×his vector (kindly provided by Günter Stier, EMBL, Germany). The primers used were: 5′-GCTACCATGGATTGTGAATCTAAACCCTTCT-3′and 5′-GCTTGCGGCCGCTTACAAGTGACTCTGATCCACATG-3′ for $Dreb2a_{168–253}$ and 5′-GCTACCATGGATTCTTCAGACATGTTTGATG-3′ and 5′-GCTTGCGGCCGCTTAGTTCTCCAGATCCAAGTAACT-3′ for $Dreb2a_{254–335}$. $Dreb2a_{168–253}$ and $Dreb2a_{245–335}$ were cloned into the pETM-6×his vector and produced as described for $Dreb2a_{168–335}$ (16). Final purification of $Dreb2a_{168–253}$ and $Dreb2a_{254–335}$ was made with ion exchange chromatography using a Mono Q 5/50 GL (GE Healthcare). The proteins were applied to the columns in 25 mM sodium phosphate buffer pH 6.2 and sodium acetate buffer pH 5.2, respectively. Both buffers contained 1 mM dithiothreitol (DTT) and a starting concentration of 20 mM NaCl. Adsorbed proteins were eluted with a linear gradient of 18 column volumes to 0.8 M NaCl on an ÄKTAexplorer (GE Healthcare). Full-length Dreb2a, $Dreb2a_{f.l.}$, was cloned into a pETM-6×his-GB1 vector at the NcoI/NotI sites and the resulting plasmid was transfected into the *Escherichia coli* Rosetta (DE3) pLysS strain. The bacteria were grown at 30°C in Terrific Broth supplemented with 100 μg/ml kanamycin and 34 μg/ml chloramphenicol. Protein expression was induced by addition of isopropyl β-D-thiogalactopyranoside (IPTG) to 1 mM at OD_{600} = 1.5. After 6 h of induction, cells were harvested by centrifugation and pellets were lysed in 20 mM Tris pH 8.0, 300 mM NaCl, 0.2% NP40 and 2 mM β-mercaptoethanol. The lysates were sonicated on ice with a Branson Sonifier 450 equipped with a microtip (VWR, Sweden). The following settings were applied: duty cycle 50%, output control 3.5, time 8 min. The lysates were then cleared by centrifugation at 35 000 *g* for 1 h using a 45Ti rotor (Beckman Coulter AB, Sweden), and $Dreb2a_{f.l.}$ was purified from the supernatant by ammonium sulfate precipitation (20%). Precipitated proteins were dissolved in 20 mM Tris pH 7.5, 100 mM NaCl and 2 mM β-mercaptoethanol and loaded onto a Mono S 5/50 GL (GE Healthcare). Adsorbed proteins were eluted with a linear gradient to 800 mM NaCl. Fractions containing $Dreb2a_{f.l.}$ were pooled, and dialyzed against 20 mM Tris pH 7.5, 150 mM NaCl and 2 mM β-mercaptoethanol.

The pET21b vector containing the human Med25–ACID domain, $hMed25_{394–543}$, was a generous gift from Patrick Cramer and Michael Sattler. The vector was transformed into *E. coli* BL21 pLysS and the bacteria were grown at 20°C in Terrific Broth supplemented with 100 μg/ml carbenicillin and 34 μg/ml chloramphenicol. Protein expression was induced at OD_{600} = 1.5 with 0.1 mM IPTG for 16 h. Cell pellets were lysed in lysis buffer (50 mM sodium phosphate pH 8.0, 300 mM NaCl, 20 mM Imidazole, 0.2% NP40, 2 mM β-mercaptoethanol). A cleared supernatant was obtained by sonication (15 s on, 30 s off, output 3.5, 2 × 8 min) and centrifugation (as described above). Protein purification was made on a Ni–NTA column (Qiagen). The column was washed twice with 10 column volumes lysis buffer and three times with wash buffer (50 mM sodium phosphate pH 8.0, 300 mM NaCl, 30 mM imidazole, 2 mM β-mercaptoethanol). Elution was made in wash buffer supplemented with 300 mM imidazole. Eluted proteins were dialyzed against 20 mM Tris pH 7.0, 50 mM NaCl, 1 mM DTT and further purified on a Mono S 5/50 GL as described above. The purified protein eluted in ∼270 mM NaCl. Fractions with purified $hMed25_{394–543}$ were pooled and aliquots were stored in −20°C before analysis. The purity of the proteins used was assayed with SDS–PAGE and Coomassie stain using Page Blue (Fermentas). The protein concentrations were initially determined with Bradford protein reagent (Fermentas) and during time of experiments confirmed by photospectrometry at A 280 nm or with a NanoDrop ND-1000 spectrophotometer (Saveen Werner).

Surface plasmon resonance analysis

Binding experiments were performed at 25°C on a Biacore3000 (GE healthcare) and analyzed with the Scrubber 2 software (BioLogic Software). Attachment of $Med25_{551–680}$ and streptavidine to a Biacore CM5 sensor chip was made with an amine coupling kit according to the recommendations from GE Healthcare. Approximately 1500 resonance units (RU) of $Med25_{551–680}$ were immobilized in 10 mM potassium phosphate buffer pH 7.0 with HBS-EP buffer as running buffer [10 mM HEPES pH 7.5, 150 mM NaCl, 3.4 mM EDTA and 0.005% non-ionic surfactant polyoxyethylenesorbitan (P2O) (GE Healthcare)]. Triplicates of decreasing concentrations of $Dreb2a_{168–335}$, $Dreb2a_{168–253}$ and $Dreb2a_{254–335}$ (8 μM with 2-fold dilutions down to 0.031 μM) were

injected at 20 µl/min for 3 min in running buffer (20 mM Tris pH 7.5, 150 mM NaCl and 1 mM DTT) and the chip was regenerated with 2 M $MgCl_2$ followed by running buffer (flow 100 µl/min, 20 µl each) between each sample. Duplicates of $Dreb2a_{f.l.}$ was injected in the same Tris-running buffer supplemented with 2 mM $MgCl_2$. Between different concentrations (3 µM down to 0.047 µM with 2-fold dilution), $Dreb2a_{f.l.}$ was washed away from the chip with a quick injection (100 µl/min) of 20 µl of regeneration buffer (50 mM NaOH, 1 M NaCl) followed by a quick inject of 20 µl running buffer. Two 29-nt long oligonucleotides, 5′-AAAGATATACTA CCGACATGAGTTCCAAA-3′ and 5′-AAAGATATAC TACTTTTATGAGTTCCAAA-3′, that contain the Dreb2a-binding sequence DRE or a mutated version of the DRE sequence from the *rd29A* promoter was used for experiments with $Dreb2a_{f.l.}$ in conjugation with DNA (16). An amount of 2, 1 and 0.5 µM $Dreb2a_{f.l.}$ were incubated with 4 µM of annealed oligonucleotides in running buffer containing 2 mM $MgCl_2$ for 10 min prior to injection. Washes were made between each injection as described for $Dreb2a_{f.l.}$ alone.

For immobilization of DNA to the sensor chip, 50 µg/ml streptavidine (Sigma Aldrich) was injected at 5 µl/min until approximately 1000 RU was reached. After blockage with ethanolamine, biotin-labeled annealed oligonucleotide (10 µM) was injected at 20 µl/min in HBS-EP buffer until 350 RU was reached. A 71-nt long oligonucleotide from the promoter region of *rd29A* (described above), labeled at the 5′-end with biotin-TEG (5′ [Btn-Tg]-CAGTTTGAAAGAAAAGGG AAAAAAAGAAAAAATAAATAAAAGATATACTA CCGACATGAGTTCCAAAAAGC-3′) was used (synthesized by Sigma Aldrich). Biotin–TEG-labeled oligonucleotides have an extra spacer with mixed polarity based on triethylene glycol that confers better binding to streptavidine than unmodified biotin. The complementary unlabeled oligonucleotide was annealed to the biotinylated oligonucleotide in 2-fold excess to achieve maximal dimerization of the biotin-labeled oligonucleotide. $Dreb2a_{f.l.}$ was injected and the chip was washed as described in the previous paragraph.

The nitrilotriacetic acid (NTA) sensor chip was subjected to 100 mM $NiCl_2$ in HBS-buffer without EDTA at 5 µl/min for 5 min to obtain a metal chelating sensor surface. After activation, $D_{f.l.}$ (6.5 µM) in HBS buffer without EDTA was injected at 5 µl/min until 1100 RU was obtained. The chip was blocked with ethanolamine and unbound Ni^{2+} was subsequently removed with 250 mM EDTA at 5 µl/min for 7 min. $HumMed25_{394–543}$ was injected from 3 µM down to 0.047 µM with 2-fold dilution in Tris running buffer supplemented with 5 mM $MgCl_2$. Between the samples, the chip was washed at 100 µl/min with 35 µl of regeneration buffer (50 mM NaOH, 1 M NaCl), 35 µl of 250 mM EDTA and finally 35 µl running buffer.

In all experiments, a reference surface that had been activated and subsequently blocked was used. As an additional reference, injection of buffer controls was made in all experiments.

Far-UV circular dichroism spectroscopy

Far-UV circular dichroism (CD) spectra were acquired on a Jasco J-720 spectropolarimeter using a quartz cuvette with a 1-mm path length. The spectra were recorded at a wavelength range of 200–300 nm with 0.5 nm data interval using a scan rate of 50 nm/min. Each spectrum was an average of five scans. Each spectrum was corrected by subtracting buffer and buffer–DNA signals, respectively, and all experiments were executed at least twice. The experiments were conducted with fixed concentrations of proteins (10 and 20 µM) in the absence and presence of specific and mutated oligonucleotides (10 µM). The molar ratio of DNA:protein was always 1:1. For protein mixture experiments with DNA, $Dreb2a_{f.l.}$ was first pre-incubated with specific or mutated DNA for 1 h at room temperature before addition of $Med25_{551–680}$. All samples were incubated in a 20 mM Tris, 150 mM NaCl, 2 mM β-mercaptoethanol, 5 mM $MgCl_2$, pH 7.5 buffer at 20°C and for CD measurements as a function of time at 4°C. For the ethylene glycol (Sigma Aldrich) samples, the final concentration was fixed to 300 mg/ml.

Gel electrophoresis mobility shift assays

The 29-nt oligonucleotides described above were annealed and the probes were labeled with ^{32}P-ATP using T4 polynucleotide kinase (Fermentas). An amount of 1 µM $Dreb2a_{f.l.}$ was incubated with the labeled probes (~20 000 cpm or 20 fmol /reaction) in 25 mM HEPES pH 7.5, 50 mM KCl, 5 mM $MgCl_2$, 10% glycerol, 1 µg/ml poly dIdC (GE Healthcare), 1 µg/µl BSA and 1 mM DTT. After incubation for 10 min at room temperature, 1 µM or 4 µM of $Med25_{551–680}$ was added and the reaction was incubated for an additional 10 min at room temperature. For competition with unlabeled probe, 1.3 µM cold probe was added at the start of the reaction. The samples were separated on a 3.5% polyacrylamide Tris–Borate–EDTA gel and the dried gel was exposed to a phosphor storage screen and imaged with a Typhoon 9400 phosphorimager (GE Healthcare).

Size exclusion chromatography

A HiLoad 16/60 Superdex 200 (GE Healthcare) was calibrated with ribonuclease A (13.7 kDa), ovalbumin (44 kDa), conalbumin (75 kDa) and aldolase (158 kDa) from the gel-calibration kits supplied by the same manufacturer. The void volume (V_o) of the column was also determined to 40 ml with blue dextran 2000. An amount of 12 µM of $Dreb2a_{f.l.}$, $Med25_{551–680}$ and $Med25_{551–680}$–GST were loaded in 500 µl. When $Dreb2a_{f.l.}$ and $Med25_{551–680}$ or $Med25_{551–680}$–GST were mixed, samples were incubated for 15 min at room temperature followed by centrifugation for 15 min at 20 000 *g* before loaded onto the column. All samples were run in 20 mM Tris pH 7.5, 150 mM NaCl and 1 mM DTT at 4°C and the proteins were separated in 0.5 ml fractions. The presence of $Dreb2a_{f.l.}$, $Med25_{551–680}$ and $Med25_{551–680}$–GST in the eluted fractions was detected using immunoblotting. The proteins were concentrated through precipitation with a 4-fold excess of acetone in −20°C over night.

Precipitated proteins were collected through centrifugation at 20 000 *g* for 15 min. Air dried pellets were dissolved in SDS-loading buffer to a final concentration of 75 mM Tris pH 6.8, 1% SDS, 10% glycerol, 0.7 M β-mercaptoethanol and 0.00125% Bromophenol blue.

To validate the interaction between Dreb2a$_{f.l.}$ and Med25$_{551–680}$–GST, samples were separated on a 10% SDS–PAGE and subjected to immunoblotting. Since the GB1-tag on Dreb2a$_{f.l.}$ is a strong immunoglobulin-binding protein, secondary antibody can be used to directly identify the GB1-Dreb2a$_{f.l.}$ protein. Thus, the 50–100 kDa part of the PVDF membrane was incubated with anti-mouse secondary antibody (1:5000) for 3 h in room temperature, washed and developed with ECL solution (all reagents from GE Healthcare). The 25–50 kDa part of the membrane was incubated with anti-GST antibody (1:2000, a generous gift from professor Sven Carlsson, Umea University, Sweden) at 4°C over night, washed and incubated with anti-rabbit antibody (1:5000, GE Healthcare, Sweden) for 1 h in room temperature. All membranes were blocked in TBST (20 mM Tris pH 7.5, 150 mM NaCl and 0.1% Tween-20) containing 5% milk for 1 h before addition of antibody. All antibodies were diluted in TBST. To verify that Med25$_{551–680}$ eluted in complex with Dreb2a$_{f.l.}$, samples were loaded on a 4–12% NuPAGE® Bis–Tris gel (Invitrogen) and run in MES SDS running buffer (50 mM Tris, 50 mM MES, 0.1% SDS and 1 mM EDTA). Proteins were visualized with Coomassie stain using PageBlue.

Formaldehyde fixation

An amount of 1 μM Dreb2a$_{f.l.}$ was mixed with Med25$_{551–680}$, Med25$_{551–680}$–GST or hMed25$_{394–543}$ (1 μM or 4 μM) for 20 min in room temperature in the same buffer as the one used for gel electrophoresis mobility shift assays (GEMSA) (25 mM HEPES pH 7.5, 50 mM KCl, 5 mM $MgCl_2$, 10% glycerol, 1 μg/ml poly dIdC 1 μg/μl BSA and 1 mM DTT). Formed complexes were cross-linked by the addition of formaldehyde to a final concentration of 0.5% for 30 min in room temperature. The cross-linked proteins were mixed with SDS-loading buffer, loaded onto a 3–8% NuPAGE® Novex Tris–Acetate gel (Invitrogen) and run in Tris–Acetate SDS-running buffer (50 mM Tris–base, 50 mM Tricine, 0.1% SDS pH 8.24). Dreb2a$_{f.l.}$ boiled for 5 min was included as a denatured control. The migration of Dreb2a$_{f.l.}$ was visualized by immunoblotting as described above.

Pull-down assays

An amount of 6 μM Dreb2a$_{f.l.}$ was bond to 15 μl IgG sepharose 6 fast flow (GE Healthcare) for 30 min in binding buffer (20 mM Tris pH 7.5, 150 mM NaCl, 2 mM β-mercaptoethanol) at room temperature. hMed25$_{394–543}$ was added to a final concentration of 6 μM and the samples were incubated for 30 min. Unbound protein were collected in flow through and the beads were washed two times in 1 ml of binding buffer containing 0.05% Tween-20. Bound proteins were extracted by addition of 1× SDS-loading buffer and boiled for 5 min. The samples were loaded on a 4–12% NuPAGE® Bis–Tris gel (Invitrogen) and run in MOPS SDS-running buffer (50 mM Tris pH 7.7, 50 mM MES, 0.1% SDS and 1 mM EDTA). The proteins were detected as described for size exclusion chromatography except that hMed25$_{394–543}$ was visualized by incubation with anti-poly His antibody (1:2000, H1029, Sigma Aldrich).

Prediction of secondary structure

The prediction of secondary structures was made with the Jpred 3 server, available at www.compbio.dundee.ac.uk/jpred. It has been reported to predict secondary structure of proteins at an accuracy of 81.5% (17).

RESULTS

The structures of the Med25–ACID domain and the C-terminal domain of Dreb2a do not change upon protein–protein interaction

We previously mapped the Med25–ACID-binding domain (BD; amino acids 551–680) of Dreb2a to the region in between the activation domain (AD) and the negative regulatory domain (NRD), (Figure 1A) (16). To investigate the binding properties of Dreb2a to Med25$_{551–680}$, three different his-tagged domains of Dreb2a (Dreb2a$_{168–335}$, Dreb2a$_{168–253}$ and Dreb2a$_{254–335}$) and GST-tagged Med25$_{551–680}$ were purified to near homogeneity as described in 'Materials and Methods' section (Figure 1A). The GST-tag of Med25$_{551–680}$ was removed by protease cleavage. A typical purification result for all proteins is shown in Supplementary Figure S1.

To determine which part of Dreb2a that is needed for binding to Med25$_{551–680}$, we performed binding studies using surface plasmon resonance (SPR). We found that only the extended C-terminal domain, Dreb2a$_{168–335}$ which includes both the BD and the AD, interacted with Med25$_{551–680}$ with significant affinity. Affinity was determined from the plateau values of binding curves for injections of various concentrations of the different domains (Figure 1B). From the analysis, the dissociation constant (K_D) was estimated to 1 μM (pH 7.5, 20°C) for the Dreb2a$_{168–335}$–Med25$_{551–680}$ interaction. The Dreb2a$_{168–335}$–Med25$_{551–680}$ interaction displayed fast kinetics, thus indicating a dynamic complex (Figure 1C). This is very similar to the K_D of 1.6 μM that was determined by isothermal titration calorimetric (ITC) assays for the human Med25 ACID domain and different domains of the VP16 transcriptional activator (18).

Using Far-UV CD, we found that the spectrum of the Dreb2a$_{168–335}$ domain indicated a lack of secondary structure for this domain in solution. The negative maximum ~200 nm implies an unstructured random coil conformation (Figure 1D). In contrast, the negative peak at 230 nm in the CD spectrum of Med25$_{551–680}$ represents contribution from aromatic residues that are in an ordered conformation (19). Notably, the interaction between Dreb2a$_{168–335}$ and Med25$_{551–680}$ did not result

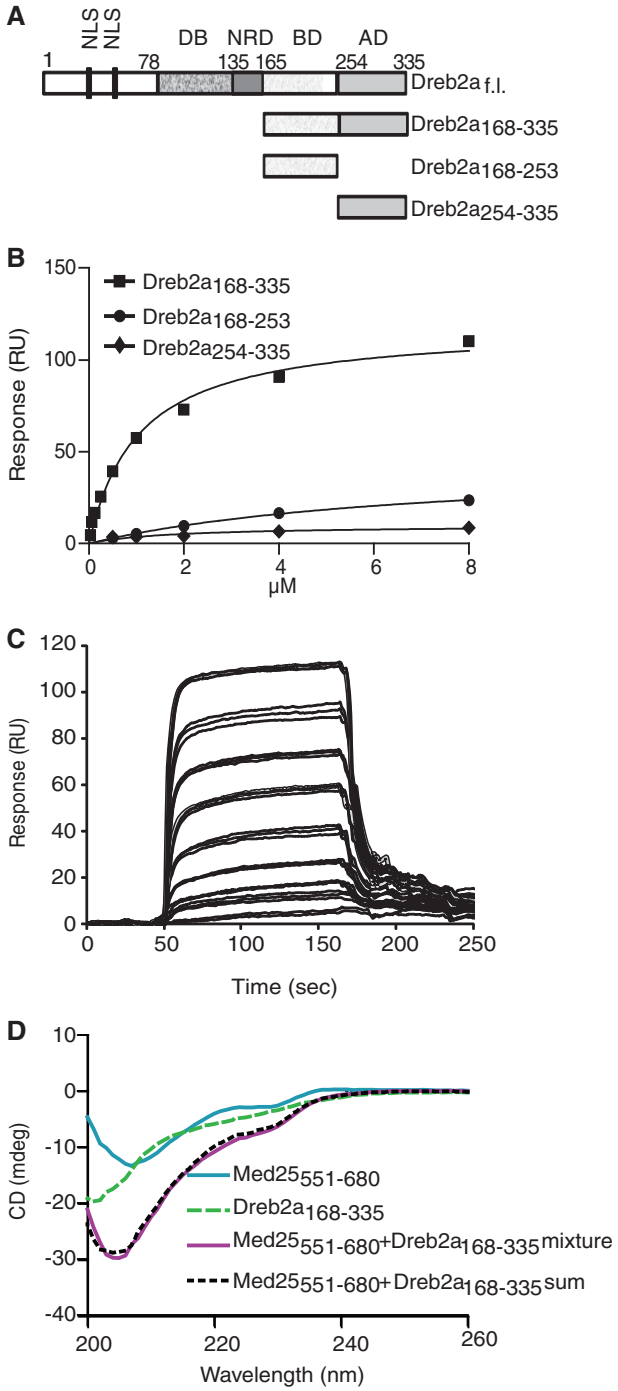

Figure 1. The C-terminal part of Dreb2a and $Med25_{551–680}$ interacts *in vitro* without affecting the protein conformations. **(A)** Schematic picture of the different domains of Dreb2a. Three truncated versions; the BD and AD ($Dreb2a_{168–335}$), the BD ($Dreb2a_{168–253}$) or AD ($Dreb2a_{254–335}$) as well as full-length ($Dreb2a_{f.l.}$) Dreb2a were used in the studies. (**B**) Increasing concentrations of the different Dreb2a domains were injected over a sensor chip to which $Med25_{551–680}$ was pre-bound. The mean of three independent plateau values are plotted. (**C**) Sensogram for the increasing concentrations of $Dreb2a_{168–335}$, showing its binding kinetics to $Med25_{551–680}$. (**D**) Far-UV CD spectra of $Med25_{551–680}$ (blue), $Dreb2a_{168–335}$ (green) and the mixture of both proteins (purple) mixed in a 1:1 molar ratio (20 μM each). Also shown is the CD sum of the individual protein signals (black dotted).

in any change in the total secondary structure content of the two proteins. The CD signal for the proteins after mixing at concentrations well above the K_D overlapped with the calculated sum of the individual CD signals for each protein (Figure 1D).

Binding of full-length Dreb2a to $Med25_{551–680}$ results in a small gain of structure

To obtain sufficient expression levels of $Dreb2a_{f.l.}$ in *E. coli*, the protein was fused to a GB1-tag along with the His-tag. The B1 IgG-BD of protein G (GB1) from *Streptococcus* is a 56 amino acids long single domain protein with one α-helix and a four-stranded β-sheet which is used as a fusion partner to increase solubility and expression of instable proteins (20,21). Due to its small size (8757.6 Da) it is regarded as one of the most optimal tags for NMR studies of instable proteins (22). Since removal of the GB1-tag from our recombinantly expressed $Dreb2a_{f.l.}$ resulted in precipitation after purification, the GB1-$Dreb2a_{f.l.}$ fusion protein of 47 kDa was purified to near homogeneity (Supplementary Figure S1B).

The interaction between $Med25_{551–680}$ and $Dreb2a_{f.l.}$ was studied using SPR, where $Med25_{551–680}$ was immobilized on a sensor chip using amine coupling. The sensograms in Figure 2A show that the interaction between $Med25_{551–680}$ and $Dreb2a_{f.l.}$ displayed complex kinetics: the dissociation was bi-phasic with a fast and a slow dissociation rate. Due to the complexity of the kinetics, an accurate K_D is difficult to determine. However, at low concentrations $Dreb2a_{f.1}$ the interaction displayed less complexity and an on rate of 22 000 M^{-1} S^{-1} could be approximated. The slow part of the dissociation rate could be approximated to 0.0023 S^{-1}. Combining the on rate and the dissociation rate gives an approximated K_D of 0.1 μM.

This dissociation rate for $Dreb2a_{f.1.,}$ is significantly slower than the dissociation rate for $Dreb2a_{168–335}$, which thus indicate that $Dreb2a_{f.l.}$, forms a more stable complex with $Med25_{551–680}$ compared to $Dreb2a_{168–335}$. Again, this K_D for the full-length Dreb2a transcription activation domain (TAD) is comparable to the K_D reported for the full-length VP16 TAD interaction with the human Med25 ACID domain (18).

Furthermore, $Dreb2a_{f.l.}$ contains more secondary structure per amino acid compared to $Dreb2a_{168–335}$, as probed by far-UV CD (Figure 2B). This is in agreement with a prediction of secondary structure content, which suggests that the N-terminal part of Dreb2a contains more α-helix and β-sheet structures (Supplementary Figure S2). Most of the predicted ordered structures are found in the DNA-BD (amino acids 78–135) that contains three β-strands and one α-helix. Moreover, mixing of $Med25_{551–680}$ and $Dreb2a_{f.l.}$ at concentrations favoring complex formation based on SPR resulted in an increased negative far-UV CD signal (~10% at 220 nm) as compared to the sum of the CD signals for the individual proteins (Figure 2C). Addition of the stabilizing osmolyte ethylene glycol to $Dreb2a_{f.1.}$ resulted in increased secondary structure based on CD measurements (~11% at 220 nm). Med25

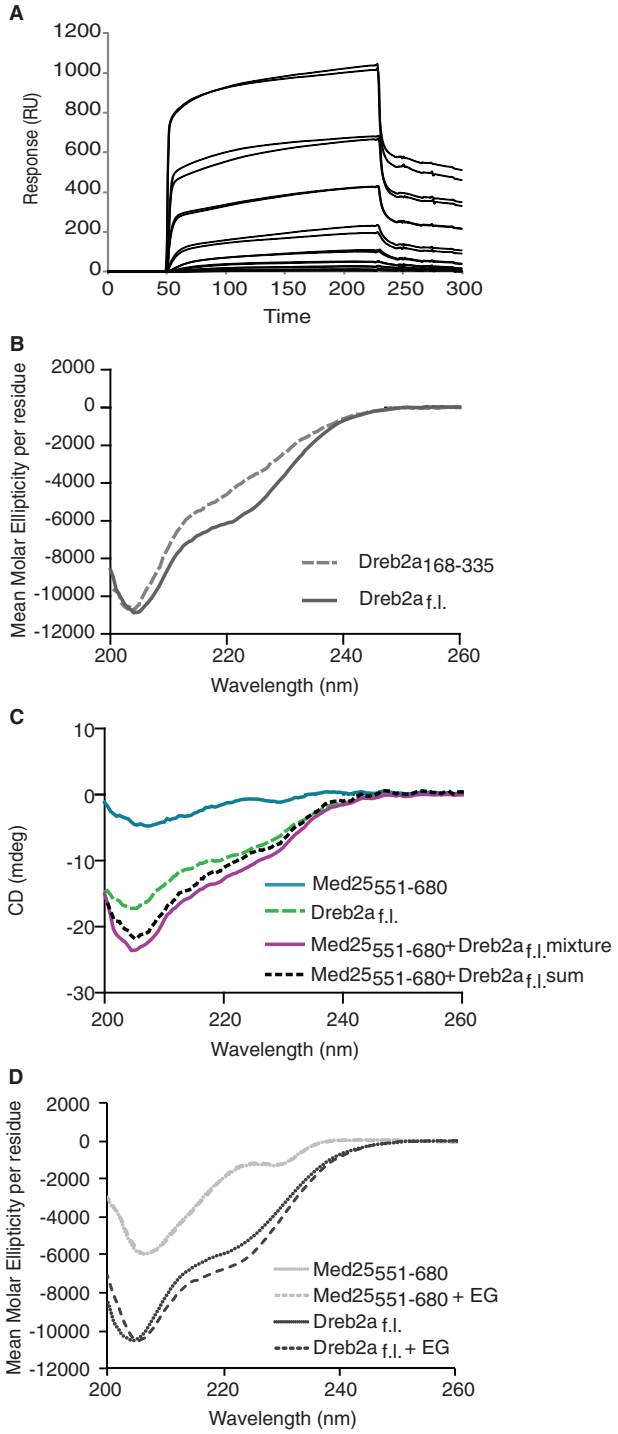

Figure 2. The interaction between full-length Dreb2a and $Med25_{551–680}$ shows complex kinetics and involves changes in secondary structure. (**A**) SRP sensograms showing the binding of increasing concentrations of $Dreb2a_{f.l.}$ to $Med25_{551–680}$. An amount of 3 μM $Dreb2a_{f.l.}$ was diluted 2-fold to 0.047 μM and duplicate samples were injected over immobilized $Med25_{551–680}$. (**B**) CD spectra of full-length Dreb2a (dark grey) and $Dreb2a_{168–335}$ domain (light grey dashed). The signals are shown as mean residue ellipticity, i.e. CD per amino acid. (**C**) CD spectra of $Med25_{551–680}$ (blue), $Dreb2a_{f.l.}$ (green) and the mixture of both proteins (purple) in a 1:1 molar ratio (10 μM). The CD spectrum of the sum of the individual proteins CD signals is also shown (black dashed). (**D**) Far-UV CD spectra of $Med25_{551–680}$ (light grey) and $Dreb2a_{f.l.}$ (dark grey) in the absence (solid) and presence (dashed) of 300 mg/ml ethylene glycol (EG).

was, however, not affected by the addition of ethylene glycol (EG) (Figure 2D). This implies that $Dreb2a_{f.l.}$ is prone to acquire a more ordered conformation under certain conditions.

Both $Dreb2a_{f.l.}$ and $Med25_{551–680}$ is present as monomers and the stoichiometry of binding to each other is 1:1

The size of $Med25_{551–680}$, $Med25_{551–680}$ –GST, $Dreb2a_{f.l.}$ and the $Med25_{551–680}$ /GST– $Dreb2a_{f.l.}$ proteins were investigated with size exclusion chromatography. $Med25_{551–680}$ –GST (42 kDa) eluted at 71 ml which corresponds to an 80-kDa globular protein when compared to a standard curve generated from separation of various standard proteins on the same gel-filtration column (Figure 3A and E). This is in agreement with other studies that indicate dimerization of GST monomers (23–25). However, GST-fusion proteins are sometimes detected as monomers (26,27), a feature that can be concentration dependent (28). $Dreb2a_{f.l.}$ that has a molecular weight of 47 kDa eluted close to 71 ml, suggesting that it either is present as an extended, non-globular monomer or as a dimer (Figure 3A and C). Complex formation of $Med25_{551–680}$ –GST and $Dreb2a_{f.l.}$ generated a shift of the peak corresponding to the elution profile of a >120 kDa protein (Figure 3A and E). This shift indicates that $Med25_{551–680}$ –GST and $Dreb2a_{f.l.}$ interact and the elution profile is most compatible with a complex composed of one $Med25_{551–680}$–GST dimer (84 kDa) and one $Dreb2a_{f.l.}$ monomer (47 kDa) when mixed in a 1:1 ratio. However, the resolution in this region is low and it is thus difficult to draw any further conclusions other than that $Med25_{551–680}$–GST and $Dreb2a_{f.l}$ form a complex. The presence of $Med25_{551–680}$ –GST and $Dreb2a_{f.l.}$ in the fractions was further confirmed with immunoblotting (Figure 3B). Moreover, when $Med25_{551–680}$ without the GST-tag was fractionated it eluted at 90.4 ml, which corresponds to the elution profile of a 16.4 kDa protein (Figure 3C and E). $Med25_{551–680}$ has a theoretical molecular weight of 14.7 kDa, thus indicating that $Med25_{551–680}$ is present as a monomer when the GST-tag is removed. Complex formation of $Dreb2a_{f.l.}$ with untagged $Med25_{551–680}$ resulted in a small shift in migration, representing an increased molecular weight of 10 kDa (Figure 3C and E). This suggests that the binding of $Med25_{551–680}$ to $Dreb2a_{f.l.}$ is 1:1 and that the $Med25_{551–680}$ interaction induces a minor change in the structure of $Dreb2a_{f.l.}$ which affects its migration on the column. The elution of $Med25_{551–680}$ at 70 ml when bound to $Dreb2a_{f.l.}$ was confirmed with immunoblotting (Figure 3D).

The size of the $Med25_{551–680}$ and $Dreb2a_{f.l.}$ complex was further investigated by formaldehyde cross-linking and SDS–PAGE. As illustrated in Figure 3F, cross-linked $Dreb2a_{f.l.}$ did not differ in size compared to non-crosslinked and denatured $Dreb2a_{f.l.}$, showing that it exists as a monomer. Cross-linking of the $Dreb2a_{f.l.}$–$Med25_{551–680}$ complex reduced the migration of $Dreb2a_{f.l.}$ with ~10 kDa, when the proteins were mixed in a 1:1 ratio. A 4-fold excess of $Med25_{551–680}$ mixed with $Dreb2a_{f.l.}$ revealed that $Dreb2a_{f.l.}$ can bind

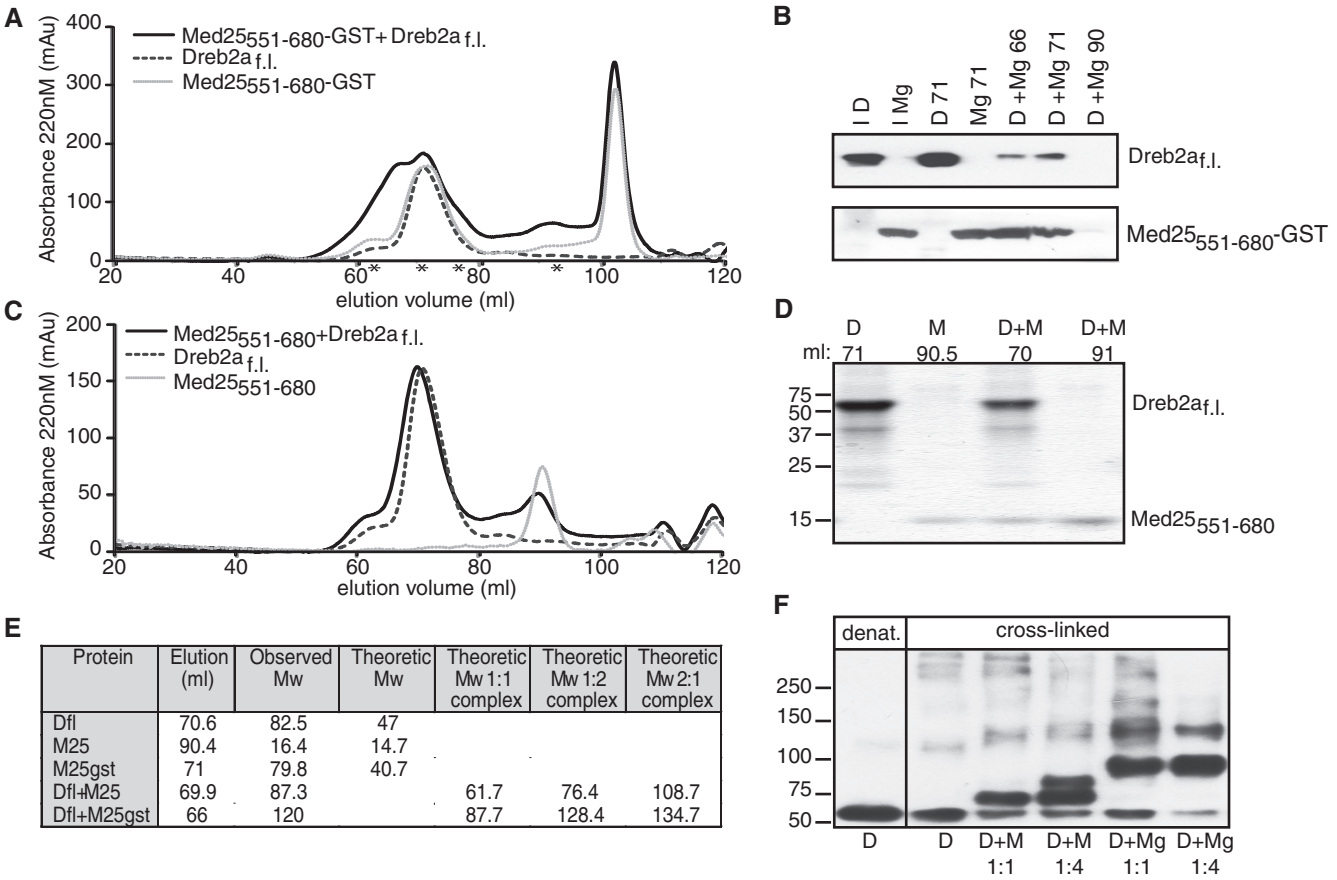

Protein	Elution (ml)	Observed Mw	Theoretic Mw	Theoretic Mw 1:1 complex	Theoretic Mw 1:2 complex	Theoretic Mw 2:1 complex
Dfl	70.6	82.5	47			
M25	90.4	16.4	14.7			
M25gst	71	79.8	40.7			
Dfl+M25	69.9	87.3		61.7	76.4	108.7
Dfl+M25gst	66	120		87.7	128.4	134.7

Figure 3. Full-length Dreb2a and $Med25_{551–680}$ bind each other mainly with a 1:1 ratio. (**A**) Size exclusion chromatogram for $Dreb2a_{f.l.}$ (dark grey) and $Med25_{551–680}$–GST (light grey) alone and in complex (black). The molecular weights of the standards used are marked with stars on the *x*-axis. (**B**) The presence of $Dreb2a_{f.l.}$ (D) and $Med25_{551–680}$**–GST** (Mg) in the eluted fractions (ml) was confirmed with immunoblot. Input (I) controls are shown in lane 1 and 2. (**C**) Size exclusion chromatogram for $Dreb2a_{f.l.}$ (dark grey) and $Med25_{551–680}$ (light grey) alone and in complex (black). (**D**) Coomassie-stained SDS–PAGE on eluted fractions (ml) show in which fractions $Dreb2a_{f.l.}$ (D) and $Med25_{551–680}$ (M) are found. (**E**) List of the observed molecular weights in A and C (calculated from the standard) compared to the theoretical molecular weights of the single proteins and possible complex formations of $Dreb2a_{f.l.}$ and Med25. Ratios of 1:1, 1:2 and 2:1 of $Dreb2a_{f.l.}$ versus Med25 are listed. (**F**) Formaldehyde cross-linked (0.5%) $Dreb2a_{f.l.}$, (D), $Med25_{551–680}$–GST (Mg) and $Med25_{551–680}$ (M) alone or in complex was separated on a 4–12% gradient gel and the migration $Dreb2a_{f.l.}$ was visualized by immunoblot. Complex formation of $Dreb2a_{f.l.}$, and $Med25_{551–680}$ was induced at 1:1 (1 μM each) and 1:4 (1 μM $Dreb2a_{f.l.}$ and 4 μM $Med25_{551–680}$) ratios. Denatured $Dreb2a_{f.l.}$, in the first lane was included as a control.

two monomers of $Med25_{551–680}$ *in vitro* when $Med25_{551–680}$ is present in excess. Cross-linking of $Dreb2a_{f.l.}$ and $Med25_{551–680}$–GST resulted in a complex at 130 kDa, showing that $Dreb2a_{f.l.}$ binds $Med25_{551–680}$–GST dimers. However, most of this mixture resulted in an elution profile corresponding to a size of 90 kDa, which illustrate that the $Dreb2a_{f.l.}$ and $Med25_{551–680}$–GST complex mainly consist of one $Dreb2a_{f.l.}$ monomer and one $Med25_{551–680}$–GST monomer. Addition of a 4-fold excess of $Med25_{551–680}$–GST did not result in an increased amount of the larger complex of 130 kDa. In summary this illustrates that $Dreb2a_{f.l.}$ and $Med25_{551–680}$ primarily binds each other in a 1:1 ratio.

The binding of $Dreb2a_{f.l.}$ to $Med25_{551–680}$ is reduced when $Dreb2a_{f.l.}$ is pre-bound to DNA

The conserved sequence TACCGACAT, named the dehydration-responsive element (DRE), is an essential *cis*-acting element for induction of *RD29A* expression in the ABA-independent response to dehydration, high salinity and cold (29). $Dreb2a_{f.l.}$ has been shown to bind sequence-specifically to the TACCGACAT sequence and not to the mutated TACTTTTAT sequence (30). We confirmed this by GEMSA and addition of $Med25_{551–680}$ resulted in a super-shift of the $Dreb2a_{f.l.}$–DNA complex (Figure 4A). This shows that DNA-bound $Dreb2a_{f.l.}$ binds $Med25_{551–680}$. Since the super-shift was very small, most likely due to the small size (14.7 kDa) and high pI (9.64) of $Med25_{551–680}$, $Dreb2a_{f.l.}$ alone was loaded both in lane 4 and 7 as controls. The binding property of $Dreb2a_{f.l.}$ to DNA was monitored with SPR where biotinylated oligonucleotides were attached to a streptavidine-coated chip. The binding curves showed that the $Dreb2a_{f.l.}$–DNA binding was dynamic, with fast on and off rates (Figure 4B). When the plateau values of the curves in Figure 4B were plotted, the K_D was determined to

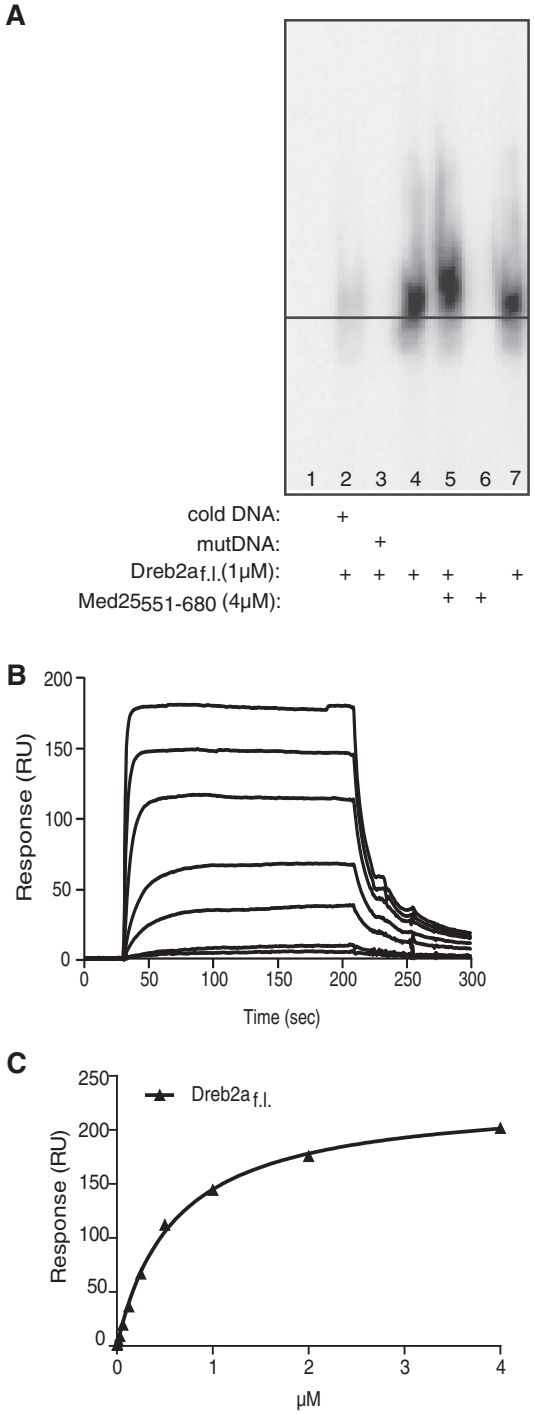

Figure 4. Dreb2a binds its specific DNA with fast kinetics. (**A**) The binding of $Dreb2a_{f.l.}$ to 29-nt oligonucleotides with the TACCGACAT sequence (Wt-probe) or the mutated TACTTTTAT sequence (mut-probe) was monitored with GEMSA. Lane 1:Labeled Wt-probe, Lane 2: Labeled Wt-probe, $Dreb2a_{f.l.}$ (1 μM), a 1000-fold molar excess of unlabeled Wt-probe, Lane 3- $Dreb2a_{f.l.}$ induced shift using labeled mut-probe, Lanes 4 and 7: Labeled Wt-probe and $Dreb2a_{f.l.}$ (1 μM), Lane 5: Labeled Wt-probe, $Dreb2a_{f.l.}$ (1 μM) and $Med25_{551–680}$ (4 μM), Lane 6: Labeled Wt-probe and $Med25_{551–680}$ (4 μM) (**B**) A biotin label oligonucleotide of 71 nt that contain the binding site TACCGACAT was immobilized on a streptavidine coated sensor chip and graded concentrations of $Dreb2a_{f.l.}$ was injected. (**C**) A streptavidine coated surface was used as reference, the plateau values were plotted and the dissociation constant was determined.

0.60 μM (Figure 4C). This K_D value is slightly higher than what was detected for the *Arabidopsis* cold-responsive transcription factor RAV_1 and the rice bZIP transcriptional activator RF2b (0.15 and 0.457 μM, respectively) (31,32). As noticed by Yamasaki *et al.*, the DNA interaction is abolished by high salt concentrations and thus, the use of different buffers can explain the difference. We found that a lower salt concentration resulted in stronger binding of $Dreb2a_{f.l.}$ to its DNA (data not shown).

A gain in secondary structure was detected when $Dreb2a_{f.l.}$ was mixed with its specific DNA but not when mixed with the mutated oligonucleotide (Figure 5A). The increase in the negative far-UV CD signal of $Dreb2a_{f.l.}$ in presence of DNA was ~17% at 205 and 220 nm of the total signal of the protein in the absence of DNA. This indicates that structural changes that increase the overall secondary structure content occure in $Dreb2a_{f.l.}$ upon DNA binding. We assume that there are no structural changes in the DNA that affects the CD signal upon protein binding. In support of this, there are no changes in the DNA signal >260 nm (where protein has no contribution) with and without protein (not shown). Binding to DNA increased the stability of $Dreb2a_{f.l.}$ as a function of time, based on CD measurements at 4°C (Figure 5B). The negative CD amplitude of $Dreb2a_{f.l.}$ in presence of its specific DNA decreased by 14% at 205 and 220 nm after 8 days incubation, while the protein in presence of mutated DNA had a CD signal decrease of 33% at 205 and 220 nm at the same time point. Decreased CD intensity may correspond to protein unfolding and/or precipitation. In any case, the results show that Dreb2a adopts a more stable conformation when it is bound to its consensus DNA-binding site. Although comparing data after 8 days of incubation does not appear biologically relevant, the low temperature used here (4°C) slows down the reactions and thus these processes would be faster at physiological conditions. Nonetheless, this experiment is only used to emphasize a relative stability difference for $Dreb2a_{f.l.}$ when in the presence of the two different DNAs.

The complex formation of $Med25_{551–680}$ and $Dreb2a_{f.l.}$ in SPR, gel filtration and CD experiments (Figures 2 and 3) clearly shows that the interaction of $Med25_{551–680}$ and $Dreb2a_{f.l.}$ is not dependent on the binding of $Dreb2a_{f.l.}$ to DNA. To investigate what impact DNA has on the $Med25_{551–680}$–$Dreb2a_{f.l.}$ binding, additional SPR and CD measurements were performed. A reduced binding of $Dreb2a_{f.l.}$ in conjugation with DNA was observed when $Med25_{551–680}$ was attached to a sensor chip with amine coupling and $Dreb2a_{f.l.}$ was injected alone or pre-bound to DNA (Figure 6A–C). This suggests that DNA-bound $Dreb2a_{f.l.}$ has lower affinity to $Med25_{551–680}$ compared to free $Dreb2a_{f.l.}$. Binding of $Med25_{551–680}$ to $Dreb2a_{f.l.}$ pre-bound to DNA did not result in any additional structural changes since the far-UV CD spectrum of the mixture and the sum of the individual protein signals of $Med25_{551–680}$ and $Dreb2a_{f.l.}$ bound to DNA overlapped (Figure 6D).

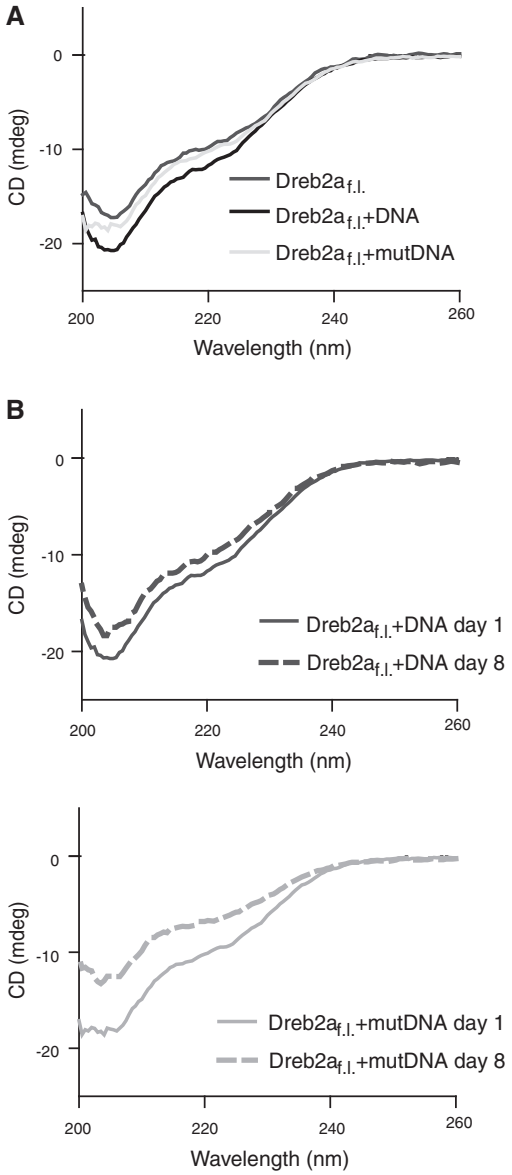

Figure 5. Interaction with DNA induces conformational changes and increased integrity of Dreb2a. (**A**) CD spectra of Dreb2a$_{f.l.}$ in the absence (dark grey) and presence of DNA (black) or mutated DNA (light grey) in a 1:1 molar ratio (10 μM). The CD signal of DNA is subtracted in both cases. (**B**) Comparison of CD spectra (DNA signal subtracted) of Dreb2a$_{f.l.}$ in the presence of specific DNA (upper) and mutated DNA (lower) at Day 1 (solid lines) and Day 8 (dashed lines) upon continuous incubation of the mixtures at 4°C.

The ACID domain of human Med25$_{394–543}$ show structural similarities to Med25$_{551–680}$ from *A. thaliana* and forms a complex with Dreb2a$_{f.l.}$

We have previously reported that there is only a week homology between the amino acid sequence of Med25 from *A. thaliana* and human (15). Interestingly, prediction of the secondary structure of the ACID domains of human Med25 (humMed25$_{394–543}$) and *A. thaliana* (Med25$_{551–680}$) revealed that some similarities exists in the distribution of α-helixes and β-sheets (Figure 7A). The NMR-structure of the human Med25 ACID domain was recently solved (18,33,34), and it was shown to contain a closed β-barrel with seven strands and three α-helixes. This is in line with the prediction of human Med25$_{394–543}$ in Figure 7A, with the expectation that the third β-sheet (B3) is predicted to be α-helical in the beginning (amino acids 447–450). The human Med25$_{394–543}$ is predicted to contain one α-helix more than Med25$_{551–680}$ and CD measurement on the two different Med25 ACIDs did indeed revealed that human Med25$_{394–543}$ contain more secondary structure (Figure 7B), Pull-down experiments with Dreb2a$_{f.l.}$ and human Med25$_{394–543}$ showed that when the proteins were mixed, a small fraction eluted together (bound) from the beads to which Dreb2a$_{f.l.}$ had been attached (Figure 7C). Most of the humMed25$_{394–543}$ did however not bind Dreb2a$_{f.l.}$ but was found in flow through. Notably, since Dreb2a$_{f.l.}$ is a plant-specific transcription factor with no apparent homolog in humans, the interaction was expected to be weak. To confirm that humMed25$_{394–543}$ interacts with Dreb2a$_{f.l.}$, cross-linking were made prior to SDS–PAGE and immunoblotting (Figure 7D). In this assay, Dreb2a$_{f.l.}$ formed a complex together with humMed25$_{394–543}$ in a similar dose-dependent manner as that detected for Med25$_{551–680}$ when mixed in 1:1 and 1:4 ratios (Figures 7D and 3F). Importantly, addition of GST did not result in complex formation with Dreb2a$_{f.l.}$. The interaction between humMed25$_{394–543}$ and D$_{f.l.}$ was studied using SPR, where His-tagged D$_{f.l.}$ was immobilized on a NTA sensor chip. The sensograms show that the interaction between humMed25$_{394–543}$ and D$_{f.l.}$ displayed similar complex kinetics as the *A. thaliana* Med25$_{551–680}$ and D$_{f.l}$ interaction (Figure 7E) and subsequently a similar dissociation constant. Due to the complexity of the kinetics, an accurate dissociation constant could not be determined but is in the same range as of Med25ACID. Detection of a humMed25$_{394–543}$–Dreb2a$_{f.l.}$ complex with three independent assays suggests that structural features that are important for interaction with activators must be conserved between Med25ACID from *A. thaliana* and humans.

DISCUSSION

Conformational disorder is found in many regulatory proteins mediating signal transduction and transcription. Disordered regions may confer advantages over folded proteins in binding and the capability of disordered protein regions to interact with multiple partners is beneficial in organizing multi-protein complexes. We had previously identified the Med25-BD in Dreb2a to amino acids 169–254 using the yeast two hybrid system (16). This domain is located between a NRD (amino acids 136–165) and an AD (amino acids 254–335) which were identified by others (35). Surprisingly, we now find that both the BD and the AD are required for interaction using purified proteins in SPR assays. A difference between the two hybrid assays and the interaction studies in this article is that the domains that are used in the two hybrid assays are expressed as fusion proteins with the Gal4 AD. It is possible that the Dreb2a BD by itself is too short to adopt

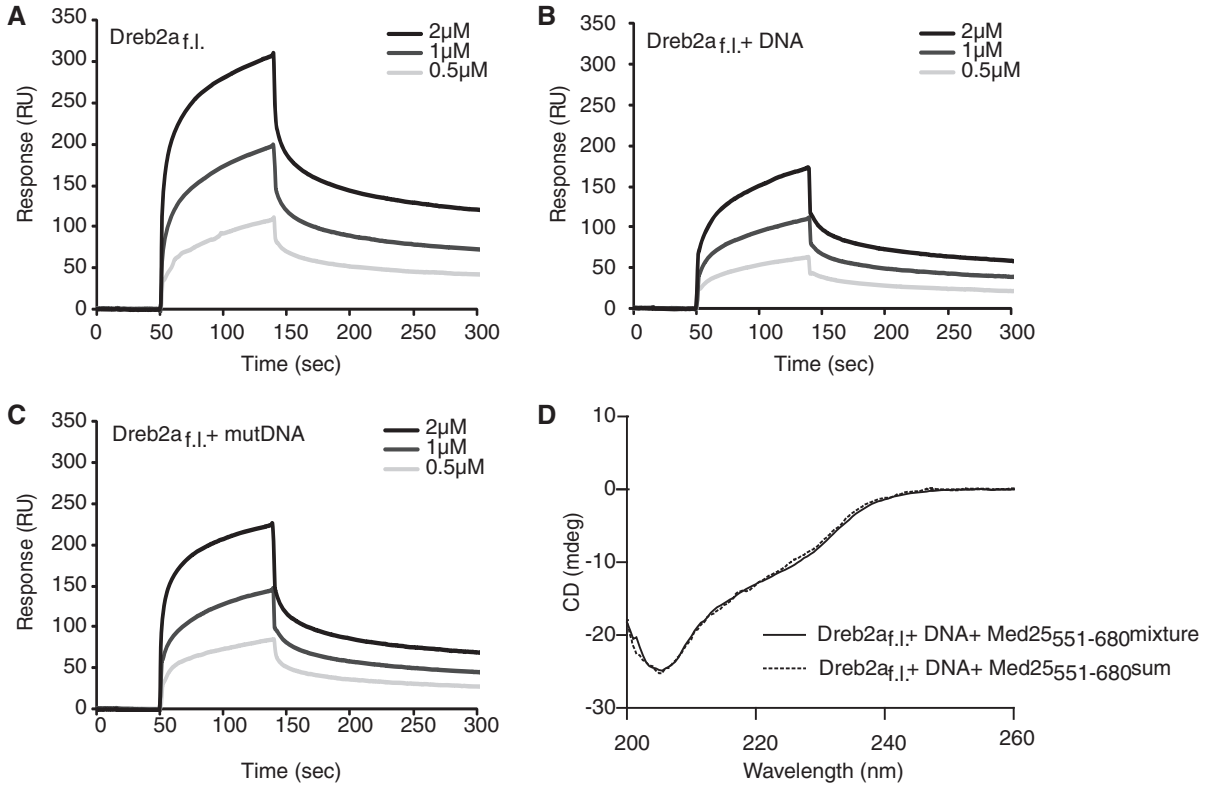

Figure 6. Dreb2a in complex with DNA show reduced binding to $Med25_{551–680}$. $Med25_{551–680}$ was attached to a sensor chip with amine coupling. (**A**) Sensogram showing dose-dependent response for $Dreb2a_{f.l.}$. (**B**) Sensogram showing dose-dependent response for $Dreb2a_{f.l.}$ pre-bound to its specific DNA and (**C**) $Dreb2a_{f.l.}$ pre-bound to the mutated DNA. **(D)** Far-UV CD spectra of a mixture of Med25 and pre-incubated Dreb2a with specific DNA (black) in a 1:1:1 molar ratio (10 μM), DNA signal subtracted. The sum of the individual CD signals of Dreb2a in presence of DNA and that of Med25 are also shown (dash).

any secondary structure, but that addition of the Gal4 AD helps to stabilize the Dreb2a BD such that it can interact with Med25. Many activator domains are known to be intrinsically unstructured in solution, which has led to the proposal of an induced fit model where flexible domains become structured upon binding to the appropriate target proteins (36). Initially we thought that this was not the case for Dreb2a, since the CD signal for the Dreb2a C-terminal domain (BD + AD) and the Med25 ACID domain after mixing overlapped with the calculated sum of the individual CD signals for each protein, thus indicating that no conformational changes occur upon binding. However, when $Dreb2a_{f.l}$ protein was used we detected an increased negative far-UV CD signal for the $Dreb2a_{f.l.}$–Med25 mixture compared to the sum of the CD signals for the individual proteins. We also found that the dissociation rate for the complex with the Med25 ACID domain was slower when using the $Dreb2a_{f.l.}$ protein relative to the $Dreb2a_{168–335,}$ which indicate a more stable complex. Thus, there are structural changes in the proteins that take place upon binding of $Dreb2a_{f.l.}$ and the Med25 ACID domain. These conformational changes may occur in both proteins or only in one of them; the CD experiments cannot resolve this issue. However, since addition of the stabilizing osmolyte ethylene glycol resulted in a gain of secondary structure of $Dreb2a_{f.l.}$ but not Med25, we speculate that the major structural changes that occur upon $Dreb2a_{f.l.}$–Med25 interaction represent changes in $Dreb2a_{f.l.}$.

The fast kinetics that we report for the Dreb2a–Med25 interaction is similar to results reported for other transcriptional activators and their interaction with different target proteins. Activator domains are typically intrinsically unstructured, such as the domains of p53, c-Myc, VP16 and the glucocorticoid receptor (37–40). Several reports show that target binding mediates folding of the unstructured domain (41,42). When target induced folding of Gal-4 and VP16 was tested with surface Plasmon resonance (43), the interaction to a set of target proteins displayed bi-phasic kinetics with a fast initial binding followed by a slower phase. This is in line with our results for the interaction between the $Dreb2a_{f.l.}$ protein and the Med25 ACID domain.

Our results using Dreb2a that has been pre bound to its cognate DNA sequence might seem counterintuitive. Figure 6 shows that Dreb2a has a lower affinity for the Med25 ACID domain in the presence of the consensus Dreb2a-binding sequence compared to when a mutated version of the sequence is present. Thus, the conformational changes that occur in Dreb2a when it binds to its consensus DNA sequence, result in a reduced binding affinity to the Med25 ACID domain. This is however what we predicted in our recently published hypothesis (16). We suggested that the conformational changes that are

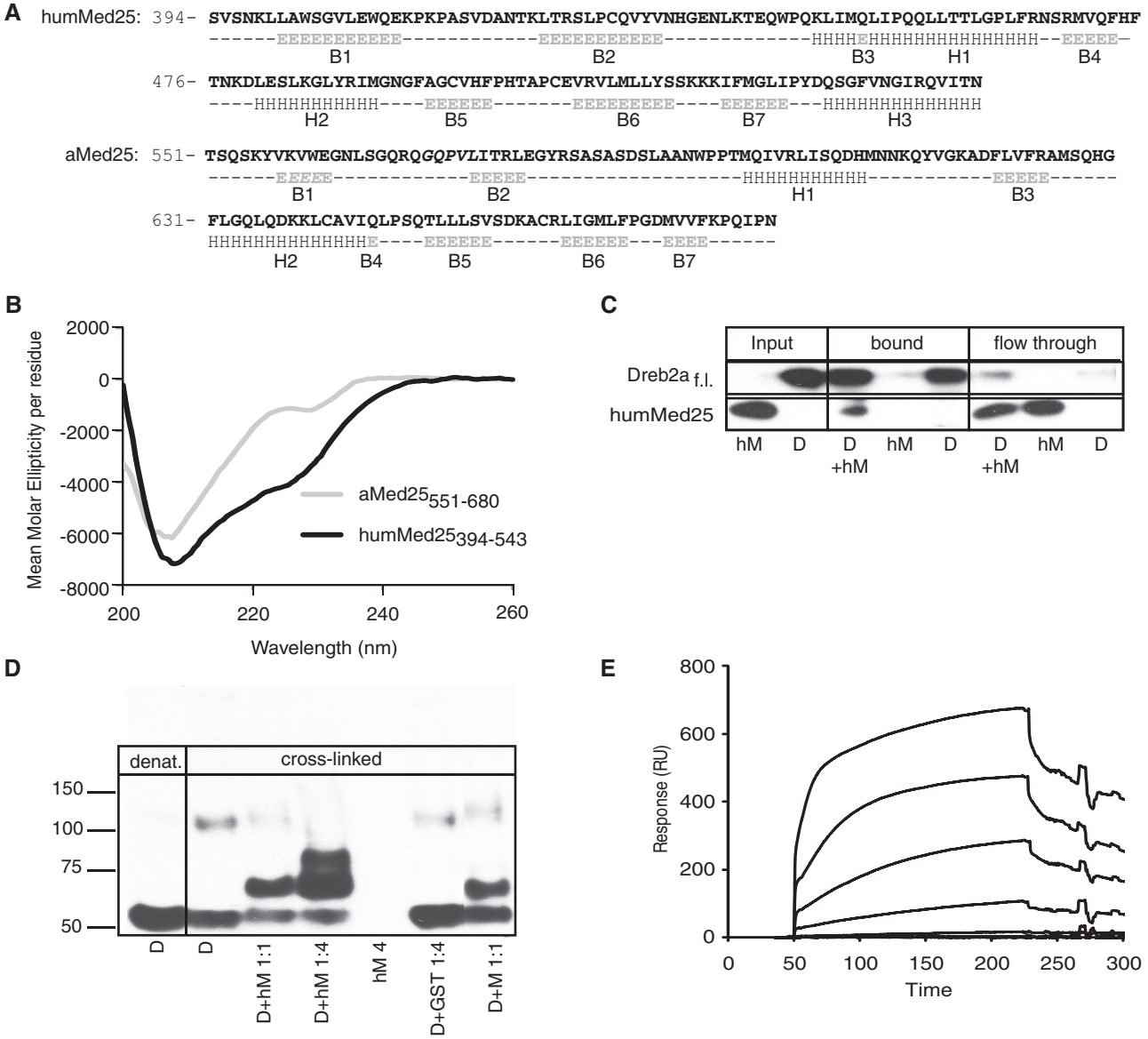

Figure 7. Structural similarity between the ACID-domains of Med25 from human and *A. thaliana* mediates similar binding propensity to Dreb2a$_{f.l.}$. (**A**) Prediction of secondary structure in the ACID-domain of Med25 from human (humMed25$_{394–543}$) and *A. thaliana* (aMed25$_{551–680}$) was made utilizing the jpred 3 server. The humMed25 contains somewhat more α-helixes (H) in dark grey and β-strands (E) in light grey than aMed25. (**B**) CD spectra of humMed25$_{394–543}$ and aMed25$_{551–680}$ confirmed that humMed25$_{394–543}$ contains more ordered structures. (**C**) Dreb2a$_{f.l.}$ (D) was bound to IgG sepharose through its GB-1 tag. Addition of humMed25$_{394–543}$ (hM) resulted in a Dreb2a$_{f.l.}$–humMed25$_{394–543}$ complex that was visualized by SDS–PAGE and immunoblotting. (**D**) Complex formation of Dreb2a$_{f.l.}$ and humMed25$_{394–543}$ (hM) was investigated with formaldehyde cross-linking (0.5%) and immunoblot. Dreb2a$_{f.l.}$, and humMed25$_{394–543}$ was mixed at 1:1 (1 μM each) and 1:4 (1 μM Dreb2a$_{f.l.}$ and 4 μM Med25) ratios. An amount of 4 μM humMed25$_{394–543}$ alone, and Dreb2a$_{f.l.}$ incubation with GST (1:4) severed as negative controls. Complex formation between 1 μM aMed25$_{551–680}$ (M) and 1 μM Dreb2a$_{f.l.}$ was included as a positive control. (**E**) SRP sensograms showing the binding of increasing concentrations of humMed25$_{394–543}$ to D$_{f.l.}$. An amount of 3 μM of humMed25$_{394–543}$ was diluted 1:1 down to 0.047 μM and samples were passed over a NTA sensor chip sensorchip where D$_{f.l.}$ was immobilized via its His-tag.

induced in Dreb2a when it binds to DNA leads to a reduced binding to the Med25 ACID domain, but an increased interaction to another mediator subunit located in the vicinity of Med25. Our hypothesis takes into consideration that Dreb2a can function both as a transcriptional activator and a transcriptional repressor based on our own functional assays in *A. thaliana* mutant lines that lack Dreb2a, on results from two hybrid experiments, and with results reported by others concerning *A. thaliana* lines where Dreb2a was overexpressed (16,30). We proposed that when interaction between the NRD of Dreb2a and Med25 is disrupted, either by deletion of the NRD of Dreb2a or by deletion of Med25, then Dreb2a functions as an activator, both for induction of genes involved in drought and in development. In contrast, we suggested that Dreb2a can execute its repressing effect of by placing its NRD in the vicinity of another mediator subunit [see the discussion in ref. (16)].

It is possible that the conformational changes in Dreb2a that would place the NRD closer to another mediator subunit, but which reduces the interaction between Dreb2a and the Med25 ACID domain are caused by interactions between Dreb2a and DNA. Further studies to identify other mediator subunits that can interact with different conformational forms of Dreb2a are required in order to verify that our hypothesis is valid. We have already identified *A. thaliana* mutants that lack other mediator subunits than Med25, but show phenotypes indicating that they are involved in the same signal pathways as Med25 (data not shown).

Finally, it is interesting to notice that the ACID domain in the human Med25 protein shows structural similarities to the Med25 ACID domain from *A. thaliana,* even if the amino acid sequences differ considerably between the two species. This structural similarity is also manifested by the interaction between Dreb2a and the human Med25 ACID domain that we detect using pull down, cross-linking and SRP assays. The ACID domain was initially identified in human Med25 due to its interaction with the herpes simplex VP16 AD. It would however be interesting to identify the natural human transcriptional regulator(s) that interacts with human Med25. Work along these lines is in progress.

SUPPLEMENTARY DATA

Supplementary Data are available at NAR Online: Supplementary Figures S1 and S2.

ACKNOWLEDGEMENTS

The authors thank Patrick Cramer and Michael Sattler for providing us with the plasmid that contains the human Med25 domain.

FUNDING

Swedish Research Council for Environment, Agricultural Sciences, and Spatial Planning (to S.B.); the Swedish Cancer Society (to S.B.); the Swedish Research Council (to S.B and P. W-S.); the Swedish Governmental Agency for Innovation Systems (to S.B.); the Kempe Foundation (to S.B. and P. W-S); the Knut and Alice Wallenberg Foundation (to P.W.-S.); the Göran Gustafsson Foundation (to P.W-S.); Umeå University Young Researcher Awards (to P.W.-S.). Funding for open access charge: Swedish Research Council.

Conflict of interest statement. None declared.

REFERENCES

1. Cantin,G.T., Stevens,J.L. and Berk,A.J. (2003) Activation domain-mediator interactions promote transcription preinitiation complex assembly on promoter DNA. *Proc. Natl Acad. Sci. USA*, **100**, 12003–12008.
2. Herbig,E., Warfield,L., Fish,L., Fishburn,J., Knutson,B.A., Moorefield,B., Pacheco,D. and Hahn,S. (2010) Mechanism of Mediator recruitment by tandem Gcn4 activation domains and three Gal11 activator-binding domains. *Mol. Cell. Biol.*, **30**, 2376–2390.
3. Fukuda,A., Nakadai,T., Shimada,M., Tsukui,T., Matsumoto,M., Nogi,Y., Meisterernst,M. and Hisatake,K. (2004) Transcriptional coactivator PC4 stimulates promoter escape and facilitates transcriptional synergy by GAL4-VP16. *Mol. Cell. Biol.*, **24**, 6525–6535.
4. Kininis,M., Isaacs,G.D., Core,L.J., Hah,N. and Kraus,W.L. (2009) Postrecruitment regulation of RNA polymerase II directs rapid signaling responses at the promoters of estrogen target genes. *Mol. Cell. Biol.*, **29**, 1123–1133.
5. Muse,G.W., Gilchrist,D.A., Nechaev,S., Shah,R., Parker,J.S., Grissom,S.F., Zeitlinger,J. and Adelman,K. (2007) RNA polymerase is poised for activation across the genome. *Nat. Genet.*, **39**, 1507–1511.
6. Rahl,P.B., Lin,C.Y., Seila,A.C., Flynn,R.A., McCuine,S., Burge,C.B., Sharp,P.A. and Young,R.A. (2010) c-Myc regulates transcriptional pause release. *Cell*, **141**, 432–445.
7. Conaway,R.C. and Conaway,J.W. (2011) Function and regulation of the Mediator complex. *Curr. Opin. Genet. Dev.*, **21**, 225–230.
8. Kim,Y.J., Björklund,S., Li,Y., Sayre,M.H. and Kornberg,R.D. (1994) A multiprotein mediator of transcriptional activation and its interaction with the C-terminal repeat domain of RNA polymerase II. *Cell*, **77**, 599–608.
9. Koleske,A.J. and Young,R.A. (1994) An RNA polymerase II holoenzyme responsive to activators. *Nature*, **368**, 466–469.
10. Bourbon,H.M., Aguilera,A., Ansari,A.Z., Asturias,F.J., Berk,A.J., Björklund,S., Blackwell,T.K., Borggrefe,T., Carey,M., Carlson,M. *et al.* (2004) A unified nomenclature for protein subunits of mediator complexes linking transcriptional regulators to RNA polymerase II. *Mol. Cell*, **14**, 553–557.
11. Bourbon,H.M. (2008) Comparative genomics supports a deep evolutionary origin for the large, four-module transcriptional mediator complex. *Nucleic Acids Res.*, **36**, 3993–4008.
12. Wands,A.M., Wang,N., Lum,J.K., Hsieh,J., Fierke,C.A. and Mapp,A.K. (2011) Transient-state kinetic analysis of transcriptional activator•DNA complexes interacting with a key coactivator. *J. Biol. Chem.*, **286**, 16238–16245.
13. Taatjes,D.J. (2010) The human mediator complex: a versatile, genome-wide regulator of transcription. *Trends Biochem. Sci.*, **35**, 315–322.
14. Meyer,K.D., Lin,S.C., Bernecky,C., Gao,Y. and Taatjes,D.J. (2010) p53 activates transcription by directing structural shifts in Mediator. *Nat. Struct. Mol. Biol.*, **17**, 753–760.
15. Bäckström,S., Elfving,N., Nilsson,R., Wingsle,G. and Björklund,S. (2007) Purification of a plant mediator from Arabidopsis thaliana identifies PFT1 as the Med25 subunit. *Mol. Cell*, **26**, 717–729.
16. Elfving,N., Davoine,C., Benlloch,R., Blomberg,J., Brännström,K., Müller,D., Nilsson,A., Ulfstedt,M., Ronne,H., Wingsle,G. *et al.* (2011) The Arabidopsis thaliana Med25 mediator subunit integrates environmental cues to control plant development. *Proc. Natl Acad. Sci. USA*, **108**, 8245–8250.
17. Cole,C.Y., Barber,J.D. and Barton,G.J. (2008) The Jpred 3 secondary structure prediction server. *Nucleic Acids Res.*, **36**, W197–W201.
18. Milbradt,A.G., Kulkarni,M., Yi,T., Takeuchi,K., Sun,Z.Y., Luna,R.E., Selenko,P., Näär,A.M. and Wagner,G. (2011) Structure of the VP16 transactivator target in the Mediator. *Nat. Struct. Mol. Biol.*, **18**, 410–415.
19. Berova,N., Nakanishi,K. and Woody,R.W. (2000) *Circular Dichroism Principles and Applications*, 2nd edn. Wiley-VCH, New York, p. 614.
20. Esposito,D. and Chatterjee,D.K. (2006) Enhancement of soluble protein expression through the use of fusion tags. *Curr. Opin. Biotechnol.*, **17**, 353–358.
21. Gronenborn,A.M., Filpula,D.R., Essig,N.Z., Achari,A., Whitlow,M., Wingfield,P.T. and Clore,G.M. (1991) A novel, highly stable fold of the immunoglobulin binding domain of streptococcal protein G. *Science*, **253**, 657–661.
22. Zhou,P. and Wagner,G. (2010) Overcoming the solubility limit with solubility-enhancement tags: successful applications in biomolecular NMR studies. *J. Biomol. NMR.*, **46**, 23–31.

23. Kaplan,W., Hüsler,P., Klump,H., Erhardt,J., Sluis-Cremer,N. and Dirr,H. (1997) Overcoming the solubility limit with solubility-enhancement tags: successful applications in biomolecular NMR studies. *Protein Sci.*, **6**, 399–406.
24. McTigue,M.A., Williams,D.R. and Tainer,J.A. (1995) Purification and crystallization of a schistosomal glutathione S-transferase. *J. Mol. Biol.*, **246**, 21–27.
25. Tudyka,T. and Skerra,A. (1997) Glutathione S-transferase can be used as a C-terminal, enzymatically active dimerization module for a recombinant protease inhibitor, and functionally secreted into the periplasm of Escherichia coli. *Protein Sci.*, **6**, 2180–2187.
26. Lim,K., Ho,J.X., Keeling,K., Gilliland,G.L., Ji,X., Rüker,F. and Carter,D.C. (1994) Three-dimensional structure of Schistosoma japonicum glutathione S-transferase fused with a six-amino acid conserved neutralizing epitope of gp41 from HIV. *Protein Sci.*, **3**, 2233–2244.
27. Bauer,M.F., Sirrenberg,C., Neupert,W. and Brunner,M. (1996) Role of Tim23 as voltage sensor and presequence receptor in protein import into mitochondria. *Cell*, **87**, 33–41.
28. Wagner,S. and Green,M.R. (1993) HTLV-I Tax protein stimulation of DNA binding of bZIP proteins by enhancing dimerization. *Science*, **262**, 395–399.
29. Yamaguchi-Shinozaki,K. and Shinozaki,K. (1994) A novel cis-acting element in an Arabidopsis gene is involved in responsiveness to drought, low-temperature, or high-salt stress. *Plant Cell*, **6**, 251–264.
30. Liu,Q., Kasuga,M., Sakuma,Y., Abe,H., Miura,S., Yamaguchi-Shinozaki,K. and Shinozaki,K. (1998) Two transcription factors, DREB1 and DREB2, with an EREBP/AP2 DNA binding domain separate two cellular signal transduction pathways in drought- and low-temperature-responsive gene expression, respectively, in Arabidopsis. *Plant Cell*, **10**, 1391–1406.
31. Yamasaki,K., Kigawa,T., Inoue,M., Tateno,M., Yamasaki,T., Yabuki,T., Aoki,M., Seki,E., Matsuda,T., Tomo,Y. *et al.* (2004) Solution structure of the B3 DNA binding domain of the Arabidopsis cold-responsive transcription factor RAV1. *Plant Cell*, **16**, 3448–3459.
32. Dai,S., Zhang,Z., Chen,S. and Beachy,R.N. (2004) RF2b, a rice bZIP transcription activator, interacts with RF2a and is involved in symptom development of rice tungro disease. *Proc. Natl Acad. Sci. USA*, **101**, 687–692.
33. Bontems,F., Verger,A., Dewitte,F., Lens,Z., Baert,J.L., Ferreira,E., de Launoit,Y., Sizun,C., Guittet,E., Villeret,V. *et al.* (2011) NMR structure of the human Mediator MED25 ACID domain. *J. Struct. Biol.*, **174**, 245–251.
34. Vojnic,E., Mourão,A., Seizl,M., Simon,B., Wenzeck,L., Larivière,L., Baumli,S., Baumgart,K., Meisterernst,M., Sattler,M. *et al.* (2011) Structure and VP16 binding of the Mediator Med25 activator interaction domain. *Nat. Struct. Mol. Biol.*, **18**, 404–409.
35. Sakuma,Y., Maruyama,K., Qin,F., Osakabe,Y., Shinozaki,K. and Yamaguchi-Shinozaki,K. (2006) Functional analysis of an Arabidopsis transcription factor, DREB2A, involved in drought-responsive gene expression. *Plant Cell*, **18**, 1292–1309.
36. Dyson,H.J. and Wright,P.E. (2002) Coupling of folding and binding for unstructured proteins. *Curr. Opin. Struct. Biol.*, **12**, 54–60.
37. Dawson,R., Müller,L., Dehner,A., Klein,C., Kessler,H. and Buchner,J. (2003) The N-terminal domain of p53 is natively unfolded. *J. Mol. Biol.*, **332**, 1131–1141.
38. Dahlman-Wright,K., Baumann,H., McEwan,I.J., Almlöf,T., Wright,A.P., Gustafsson,J.A. and Härd,T. (1995) Structural characterization of a minimal functional transactivation domain from the human glucocorticoid receptor. *Proc. Natl Acad. Sci. USA*, **92**, 1699–1703.
39. Dahlman-Wright,K., Ford,J. and Wright,A.P. (1996) Functional interaction of the c-Myc transactivation domain with the TATA binding protein: evidence for an induced fit model of transactivation domain folding. *Biochemistry*, **35**, 9584–9593.
40. Donaldson,L. and Capone,J.P. (1992) Purification and characterization of the carboxyl-terminal transactivation domain of Vmw65 from herpes simplex virus type 1. *J. Biol. Chem.*, **267**, 1411–1413.
41. Uesugi,M., Nyanquile,O., Lu,H., Levine,A.J. and Verdine,G.L. (1997) Induced alpha helix in the VP16 activation domain upon binding to a human TAF. *Science*, **277**, 1310–1313.
42. Wright,P.E. and Dyson,J.H. (2009) Linking folding and binding. *Curr. Opin. Struct. Biol.*, **19**, 31–38.
43. Ferreira,M.E., Hermann,S., Prochasson,P., Workman,J.L., Berndt,K.D. and Wright,A.P. (2005) Mechanism of transcription factor recruitment by acidic activators. *J. Biol. Chem.*, **280**, 21779–21784.